Acta Physicae Superficierum • Vol. XII • 2012

TWENTY YEARS OF MAGNETIC NANOSTRUCTURES STUDIES IN BIAŁYSTOK

A. MAZIEWSKI, W. DOBROGOWSKI, R. GIENIUSZ, J. KISIELEWSKI
M. KISIELEWSKI, Z. KURANT, P. MAZALSKI
A. STUPAKIEWICZ, M. TEKIELAK

Faculty of Physics, University of Białystok
Lipowa 41, PL-15-424 Białystok, Poland
e-mail: magnet@uwb.edu.pl

Abstract. Review of results of selected experimental and theoretical studies of magnetic nanostructures (mainly based on cobalt films) is presented. Different magneto-optical methods, developed for these investigations, are discussed. Tuning of magnetic properties by the following agents: (i) adjustment of chemical composition of layers surronding Co-layer; (ii) changes of buffer structure; (iii) post growth treatment by either ion or light irradiation, is reported. Giant Co-thickness-induced-changes of domain structure are described by an analytical approach and micromagnetic simulations. Magnetization spatial distributions are discussed for both single magnetic layers and multilayers. Special attention is paid to conditions of transitions between in-plane and out-of-plane magnetization states.

1. Introduction

Studies of magnetic materials have an almost forty year history in the team of the Department of the Physics of Magnetism in Białystok. Early investigations were focused on studying the magnetic properties of thin magnetic films, mainly garnets. Twenty years ago, nanomagnetism was selected as our new main research topic. Cooperation with Jacques Ferrés group from the University Paris-Sud in Orsay (France) was important for both launching and extending the nanomagnetism research. Since 1992 many persons from the Białystok team have had research visits in Orsay and, reciprocally, French coworkers have visited Białystok. Our nanomagnetism studies were well accelerated in the last 10 years because of cooperation, within the Polish National Scientific Network, with other Polish

teams, especially from Warszawa, Poznań, and Kraków, see Fig. 1. Progress of the nanomagnetism development in our team is connected with the realization of different European projects, see Fig. 1.

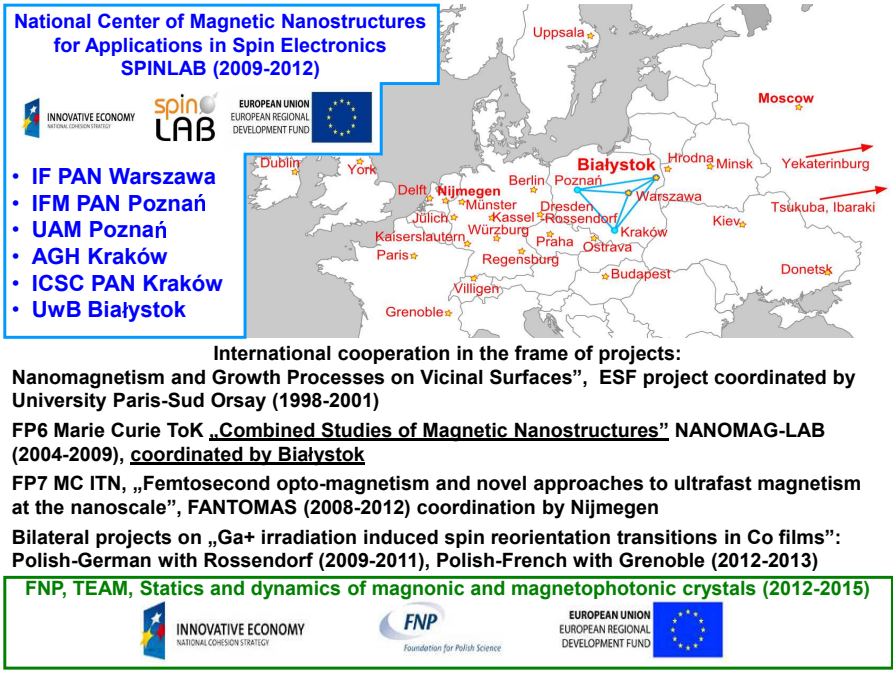

International cooperation in the frame of projects:

Nanomagnetism and Growth Processes on Vicinal Surfaces", ESF project coordinated by University Paris-Sud Orsay (1998-2001)

FP6 Marie Curie ToK „Combined Studies of Magnetic Nanostructures" NANOMAG-LAB (2004-2009), coordinated by Białystok

FP7 MC ITN, „Femtosecond opto-magnetism and novel approaches to ultrafast magnetism at the nanoscale", FANTOMAS (2008-2012) coordination by Nijmegen

Bilateral projects on „Ga+ irradiation induced spin reorientation transitions in Co films": Polish-German with Rossendorf (2009-2011), Polish-French with Grenoble (2012-2013)

FNP, TEAM, Statics and dynamics of magnonic and magnetophotonic crystals (2012-2015)

INNOVATIVE ECONOMY NATIONAL COHESION STRATEGY
FNP Foundation for Polish Science
EUROPEAN UNION EUROPEAN REGIONAL DEVELOPMENT FUND

Fig. 1: Cooperation map of the nanomagnetism studies performed by the Białystok team.

Since the 1970s, seventies, magneto-optical techniques have been a major focus of our team in Białystok. The last 20 years have seen the development of special magnetooptical methods for studies of magnetic nanostructures. These magneto-optical techniques are discussed in Chapter 2, as well as new methods used more recently in Białystok, such as scanning probe microscopy (SPM) and magnetooptical techniques by using of femtosecond laser pulses and Brillouin light scattering (BLS) spectroscopy.

Chapter 3 shows the results of the modification of magnetic and optical properties of nanostructures during growth processes and post-growth treatment. Simple systems – i.e. ultrathin single magnetic films – were mainly studied for this purpose.

Modification of magnetic ordering in ultrathin magnetic films is discussed in Chapter 4. We began our experimental and theoretical studies with simple systems – an ultrathin magnetic single layer, then with more complicated multilayers and patterned nanostructures.

2. Experimental techniques

The static and dynamic properties of magnetic nanostructures are studied ex-situ using mainly magneto-optical methods developed at Białystok. Additionally we use: (i) scanning probe microscope (SPM) with different measurement options such as magnetic force microscope (MFM) (enabling measurements in external magnetic field), atomic force microscope (AFM); (ii) ferromagnetic resonance X-band spectrometer at a frequency of 9.5 GHz. Some results obtained using these additional techniques were presented in our papers [1, 2, 3].

Magneto-optical magnetometers

We have developed in Białystok different magneto-optical effects (Kerr or Faraday) based magnetometers. These techniques are used mainly for magnetic nanostructures static or quasistatic studies as a function of both perpendicular $H_\perp$ and in-plane $H_\parallel$ applied magnetic field, see Fig. 2. Polar magnetooptical Kerr effect (P-MOKE) and longitudinal magneto-optical Kerr effect (L-MOKE) enable local detection of perpendicular and in-plane magnetization components, respectively. A sample is locally investigated analyzing images from a polarized light microscope or using a focused laser beam and single light detector.

The magneto-optical polarizing microscope is based on: (i) either home-made optical microscope constructions or a specially modified Carl Zeiss JenaPol wide-field optical polarizing microscopes enabling high-resolution imaging (Figs 2A, B); (ii) a sensitive CCD camera; (iii) software for both acquisition correlated with magnetic field changes, and processing of images. A P-MOKE remnant image, registered at zero magnetic field after sample saturation by $H_\perp$ field, is a very useful tool for studies of magnetic ordering (out-of-plane magnetization state), depending on different parameters, such as magnetic film thickness and the structure of the overlayer and underlayer, see Figs 5, 6. One can distinguish the following regions in these figures: (i) an easy magnetization axis state – the white area; (ii) the in-plane magnetization state – the black area for higher Co thickness; (iii) the superparamagnetic state – the black area for lower Co thickness. Local analysis of magnetization curves (obtained from images registered in different magnetic fields) is useful for the distinguishing of different magnetic states. There are some examples of images of the domain structure, registered at the geometry of: P-MOKE (Fig. 5A – dotted lines, Figs 6B, 7, 8C, 9) and L-MOKE (Fig. 11A).

The magneto-optical magnetometer (Fig. 2C), in either P-MOKE or L-MOKE geometries, uses: (i) laser light, which is usually focused on the sample into a spot with about 0.3 mm diameter; (ii) a standard modulation technique with a photoelastic modulator and lock-in amplifier, which enables determination of both Kerr rotation and ellipticity; and (iii) computer control: for movement of the sample for $x - y$ scanning or rotation, changes of the external magnetic field, and

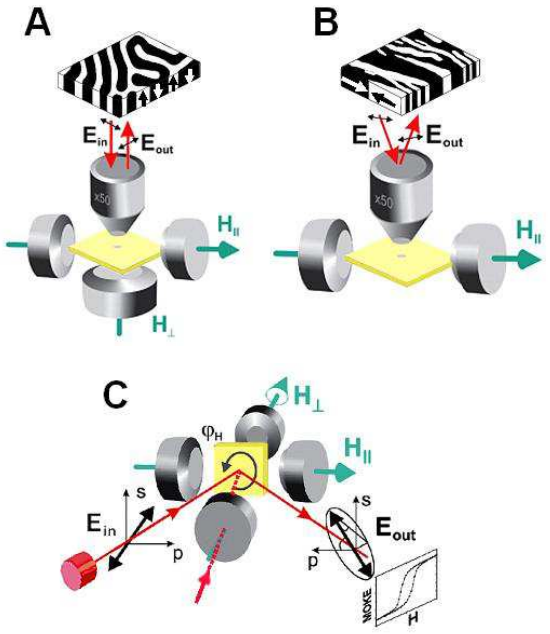

Fig. 2: Schemes of: (A, B) magneto-optical microscope with P-MOKE and L-MOKE configurations; C) magneto-optical magnetometer in L-MOKE geometry; a computer controlled sample: (i) orientation – by changing the φ_H angle in relation to the in-plane applied field $H_{\parallel}$; or (ii) changing the $x-y$ position in relation to the laser beam – $x-y$ scanning; P-MOKE geometry is also possible with illumination perpendicular to sample plane, using e.g. a hole in the gap of an electromagnet generating $H_{\perp}$ field.

data acquisition. All three magnetization components could be measured either in the same geometry or with an appropriate adjustment of the angle of incidence. Examples of results obtained by the magnetometer are presented in Fig. 8B [4].

Femtosecond laser-based magnetooptical techniques

The magneto-optical techniques based on a femtosecond laser enable studies of (i) ultrafast magnetization dynamics and (ii) the magnetization-induced second-harmonic generation (MSHG).

Ultrafast pump-probe magnetization dynamics is measured using femtosecond (35 fs) pulses from a Ti:Sapphire laser system with amplifier (Ace, Spectra-Physics) at a repetition rate of 1 kHz. These pulses are split into two parts using a beam splitter. The most intense part (pump pulse) is incident on the sample at near normal incidence. The magnetization dynamics induced by these pump pulses is followed in time by measuring the Kerr or Faraday rotation of the time

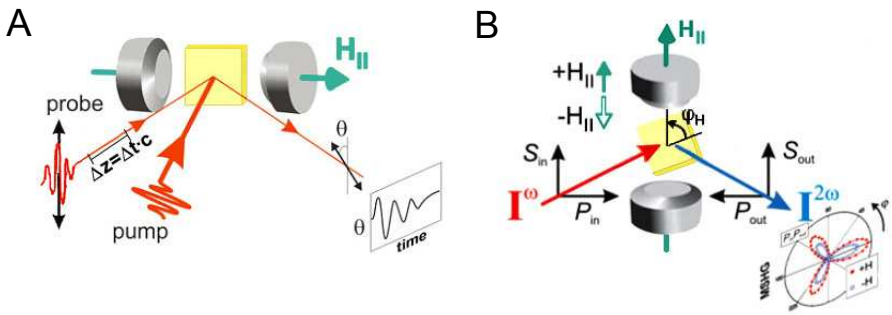

Fig. 3: Scheme of: A) ultrafast magnetization dynamics – pump-probe P-MOKE configuration; B) MSHG measurements configuration. The incoming and outgoing light polarizations component are defined.

delayed and much weaker probe pulses. Usually, the rate of pump/probe intensities is about 100. The probe pulses delay time Δt (in relation to pump ones) is tuned changing pump-probe optical paths, see Fig. 3A. The rotation angle is proportional to the projection of the magnetization vector along the wave vector of the probe light. The ultrafast magnetization dynamics studies in different magnetic systems induced by laser heating and by polarized laser light have been recently reported [5, 6].

The MSHG measurements are performed using a mode-locked Ti-sapphire (MaiTai, Spectra-Physics) femtosecond laser operating in the 690–1040 nm range with 150 fs pulse width of the laser and 80 MHz repetition rate. The reflected MSHG signal is detected by a cooled photomultiplier using a photon counting technique after special filtering to reject the fundamental wavelength. We apply an in-plane magnetic field $H_{\|}$ in a transverse magneto-optical configuration which saturates the in-plane magnetization in our samples. The MSHG intensity is recorded for various input-output polarization combinations ($P_{\mathrm{in}}P_{\mathrm{out}}$, $S_{\mathrm{in}}P_{\mathrm{out}}$, $P_{\mathrm{in}}S_{\mathrm{out}}$, and $S_{\mathrm{in}}S_{\mathrm{out}}$), at various azimuthal angles φ_H within 0–360° range, see inset in Fig. 3B. In addition, the MSHG intensity for selected values of azimuthal angles φ_H and polarization combinations are recorded. Such sets of measurements enable separation of the crystallographic and magnetic contributions to the total signal. Results of the MSHG rotational anisotropy studies of ultrathin Co films grown on a vicinal Si substrate with and without a Cu buffer layer were reported on [1].

Brillouin light scattering spectrometry

Brillouin light scattering spectroscopy is an optical method for measuring excitations in the range of frequencies from 2 GHz to 500 GHz. The fundamental

principle of BLS spectroscopy is the inelastic scattering of monochromatic light from phonons or magnons. In a classical treatment, the nature of BLS can be understood as a scattering of light from a propagating phase grating, generated, due to magneto-optical effects, in the magnetic material by spin waves. The laser light is Braggs reflected from the phase grating, with its frequency being Doppler-effect shifted by the spin wave frequency. As BLS is an optical technique, it allows for local measurement of spin waves with a spatial resolution defined by the diameter of the laser spot, typically of the order of 40 μm. Thermally excited, both magnons and phonons are usually studied by BLS. As an example of conventional BLS system application, magnetic and elastic properties in trilayer Mo/Co/Au systems [2] were investigated in the backscattering geometry. A wide recent extension of modern BLS systems is connected with the development [7, 8] of: (i) microBLS (μBLS) spectrometers with the spatial resolution increased into the submicrometer range; (ii) time and space resolved BLS spectrometers for spin-waves investigation based on magnetization excitation by microwave pulses. Our BLS system allows both these modern options.

With the aim of investigating both the spatial and temporal properties of spin wave packets, we use the BLS setup schematically shown in Fig. 4 (where, as an example, the forward scattering geometry is illustrated). Light from a frequency-stabilized-solid-state laser in single mode operation with a wavelength of $\lambda = 532\,\mathrm{nm}$ and typical linewidth $\Delta\nu = 20\,\mathrm{MHz}$, is focused onto the sample. The light inelastically scattered from the spin waves is collected and passed to a Sandercock's-type, six-pass, tandem Fabry-Perot interferometer. The light is detected by either a photomultiplier or an avalanche photodiode. Either a computer or a multichannel analyzer collects the photon signals as a function of the mirror spacing and displays the data. Spin waves with a frequency ν are generated by a microwave input antenna. The spatial distribution is measured by scanning the laser beam across the sample and recording the scattering intensity which is proportional to the spin wave intensity, at different points in the sample.

The laser beam is focused almost down to 250 nm in our μBLS and the scattered light can be effectively collected from this small area. The sample is mounted on an xyz piezoelectric stage, which allows sample scanning along all three dimensions with a precision of about 20 nm. For visualization of the position of the laser spot on the surface of the sample, and to keep it in the same place, we use a system with an active beam stabilization technique. The μBLS has been used to measure the magnetic dynamics of patterned samples and in micrometer isolated magnetic elements, such as stripes, squares, rectangles, circles, rings, and ellipses. As an example, the effect of intense microwave-magnetic-field-induced resonant-nonlinear-frequency multiplication in sub-micrometer sized Permalloy elliptical dots was investigated in our paper [9].

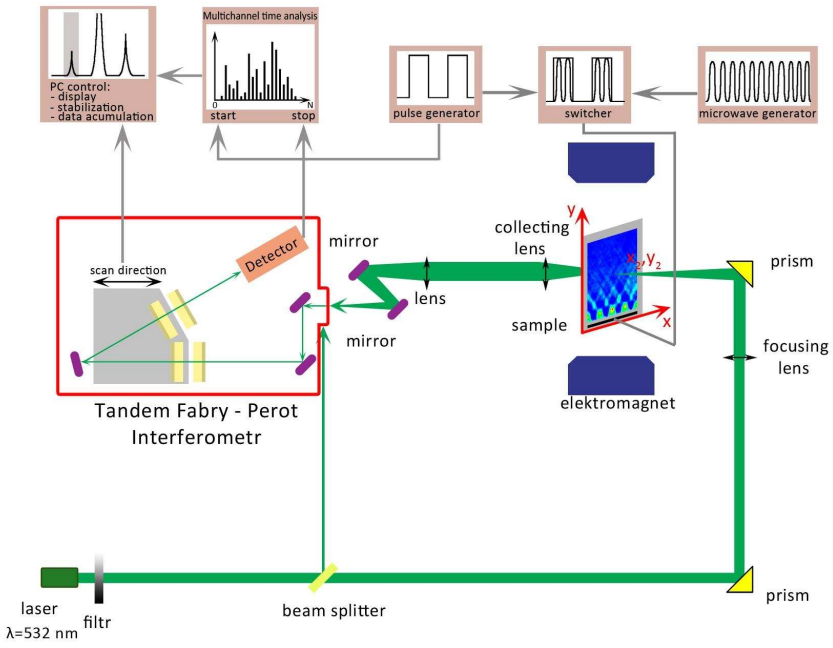

Fig. 4: Scheme of BLS spectrometer with time and space resolution.

3. Changes of magnetic properties of ultrathin Co film during the growth process and after sample deposition

The discussion below is focused mainly on changes of magnetic anisotropy driven by different factors.

Let us consider the following simple form of magnetic anisotropy:

$$E_A = \left(-2\pi M^2 + K_{1\mathrm{V}} + \frac{K_{1\mathrm{SU}} + K_{1\mathrm{SB}}}{d}\right) \sin^2\theta = K_{1\mathrm{eff}} \sin^2\theta \qquad (1)$$

where θ is the angle between magnetization and sample normal; d is the thickness of the magnetic film; $K_{1\mathrm{V}}$, $K_{1\mathrm{SB}}$ and $K_{1\mathrm{SU}}$ are volume, buffer-surface, and upper-surface contributions to magnetic anisotropy, respectively; and the first term in the bracket is the demagnetization factor. While decreasing film thickness below d_{RPT} (d_{RPT} is defined by $K_{1\mathrm{eff}}\,(d_{\mathrm{RPT}}) = 0$, or after Eq. 1 $d_{\mathrm{RPT}} = 2K_{1S}/(2\pi M^2 - K_{1\mathrm{V}})$), magnetization evolves from in-plane into perpendicular state in the reorientation phase transition RPT region.

Co properties modifications by overlayer and underlayer compositions

We have experimentally studied the influence of both nonferromagnetic overlayers and buffer layers on the RPT in Co single layers, see Figs 5 and 6. Cobalt was deposited by MBE in a wedge shape along the "x" axis. The critical thickness d_{RPT} of about 1.8 nm and 1.3 nm was found for Au/Co/Au and Au/Co/Ag layers, respectively, see Fig. 5A. Domain structures were created by applying a pulse of $H_{\perp}$ to the sample, which previously had been saturated in the opposite direction. Wall positions, determined for a few values of $H_{\perp}$ amplitude, are marked in Fig. 5A by dots. Analysis of the domain wall position enabled determination of the spatial distribution of the coercivity field, see Fig. 5B. A roughly 1 nm-thick silver overlayer was found to be enough to change substantially magnetic anisotropy and coercivity.

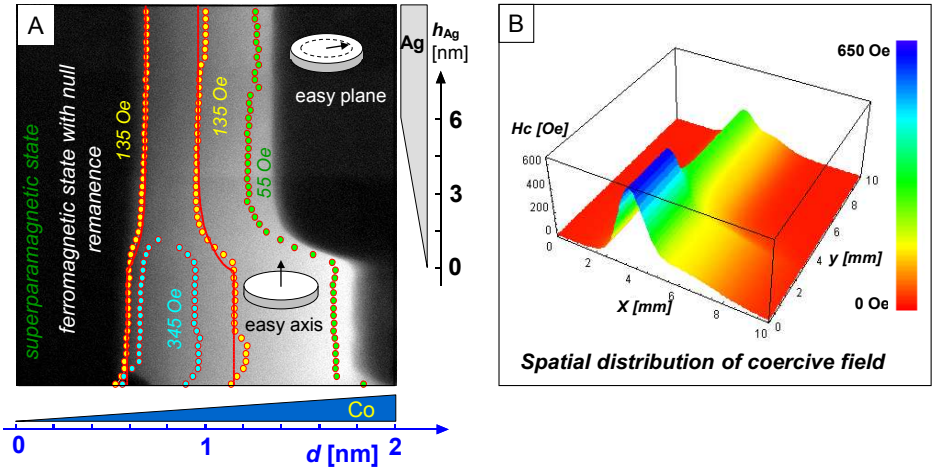

Fig. 5: A) PMOKE remnant image of the double wedge nanostructure deposited on $10 \times 10\,\mathrm{mm}^2$ large sapphire substrate: (i) Au buffer; (ii) Co wedge from 0 to 2 nm along the "x" axis; (iii) Ag wedge along the "y" axis from 0 at $y = 3$ mm to 6 nm at $y = 7$ mm; Ag flat, 6 nm thick, from $y = 7$ until $y = 10$ mm; (iv) Au 8 nm thick overlayer. Positions of the domain wall, detected for different applied magnetic field, are indicated by dotted lines. B) Reconstructed spatial distribution of the coercivity field [10, 11].

An example of the influence of different surroundings on Co magnetic ordering is shown in Fig. 6. A Co wedge (along the "x" axis) was sandwiched in three zones spread along the "y" axis as follows: Mo/Co/Au, Au/Co/Au and Au/Co/Mo. By considering both that the RPT, magnetic anisotropy of the Mo/Co/Au, and the Au/Co/Mo structures are not equivalent, and Eq. 1, then one can deduce the influence of different growth conditions on magnetic anisotropy resulting e.g. on different contributions of the volume anisotropy in both cases. A needle-like

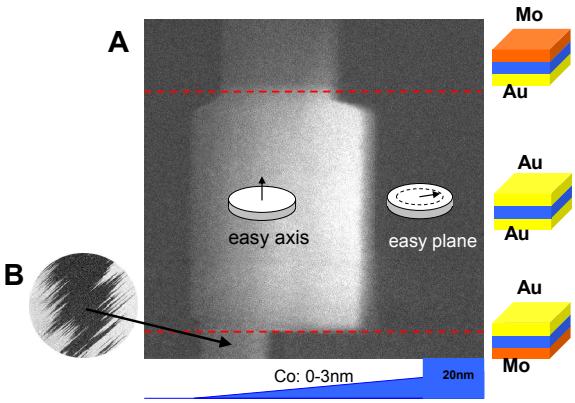

Fig. 6: A) P-MOKE remnant image of cobalt wedge (along "x" axis) with different surrounding zones: Mo and Au, Au and Au; Au and Mo; B) image of domain structure from this region where Co is deposited on Mo and covered by Au.

domain structure was observed in Co films deposited on a Mo buffer [12, 13]. This unusual domain geometry is connected with a large in-plane magnetic anisotropy, deduced from both magnetooptical magnetometry and FMR studies [14, 15].

Co properties modifications by vicinal substrates

The influence of substrate morphology and geometry on nanostructures' magnetic properties [1, 16, 17] was studied using a vicinal substrate (Al_2O_3, Mo, W, Si) with a stepped structure (either single atomic steps or step bunches) as a template for the growth of ultrathin Co films with different buffer layers (Mo, Cu, Au). All the samples were capped with a Au protective layer enabling an ex-situ study. The samples were prepared by molecular beam epitaxy (MBE) in an ultra-high vacuum system. The surface and structure properties of the layers were monitored in-situ by electron diffractions (LEED and RHEED) and by scanning tunneling microscopy (STM). Magnetic and optics measurements have been performed ex-situ at room temperature by means of ferromagnetic resonance, magneto-optical Kerr effect based magnetometer, and optical microscopy.

The modification of the magnetocrystalline and step-induced magnetic anisotropies in a configuration of Co/Si and Co/Cu films has been observed [1]. The vicinal substrate induced the out-of-plane magnetization state, and magnetization reorientation transition from perpendicular to in-plane magnetization orientation, was observed for a wide range (1–8 nm) of Co thicknesses and for different geometry of the W and Mo substrates [16, 17] (see Fig. 7). The experiments reveal a strong increase of the magnetic domain wall velocity, about 2 orders of magnitude, for 3 monolayer Co films with higher step-density of Si substrate [18].

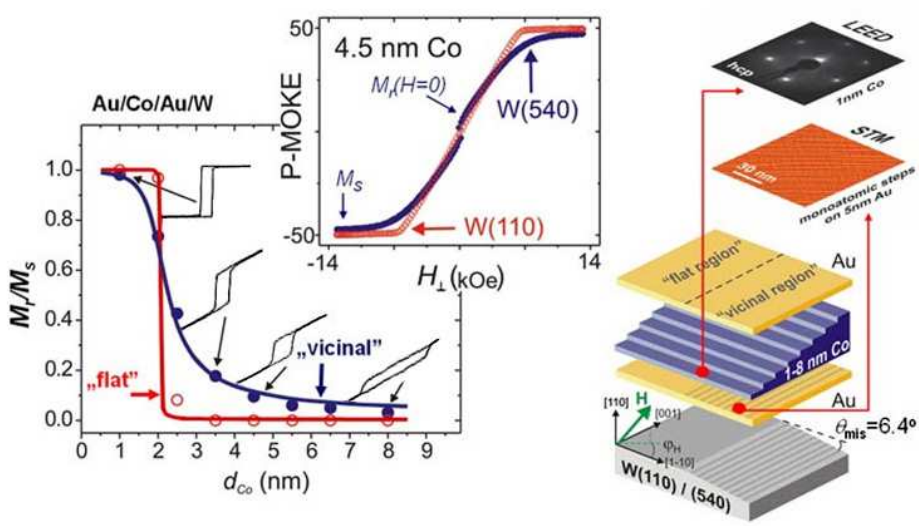

Fig. 7: Dependence of out-of-plane magnetization component Mr/Ms on the Co thickness for W(110) (open points) and W(540) (full points) substrate regions. Solid lines are calculated within the theoretical model [16]. Insets: the hysteresis loops for the 4.5 nm thick Co film on both the flat and vicinal region measured by P-MOKE and schematic configuration of the sample with STM and LEED results [16].

Co properties modifications by ions and light irradiation

Above, we have shown some examples of changes of Co properties during the growth process. Post-growth modifications of properties are also possible, using e.g. irradiation by ions or by light. Usually, irradiation of nanostructures induces a degradation of interfaces and a decrease of contribution of surface anisotropy, which finally results in a decrease of magnetic anisotropy [19]. Contrary to this, we have presented opportunities to increase the magnetic anisotropy by Ga-irradiation [3, 4] of Pt/Co/Pt nanostructures. Fig. 8A shows a two-dimensional diagram (where d is the Co thickness and F is the Ga^+ fluence) of remnant rotation θ_{REM}, determined locally using the magneto-optical magnetometer. θ_{REM} amplitude is marked in colors. The RPT, the transition between blue and red regions, occurs for Co thickness d_{RPT} equal to about 2.4 nm in the reference, non-irradiated, region ($y < 2$ mm). The two Ga-irradiation-induced, out-of-plane magnetization branches are well visible for a wide range of d and F. The appearance of these branches can be explained by Ga-fluence-driven creation of phases of a Co-Pt alloy with high magnetic anisotropy [4]. A superparamagnetic region (violet area) is visible at the top left corner of the diagram. Ga-fluence-induced increase of Kerr rotation was also observed [4].

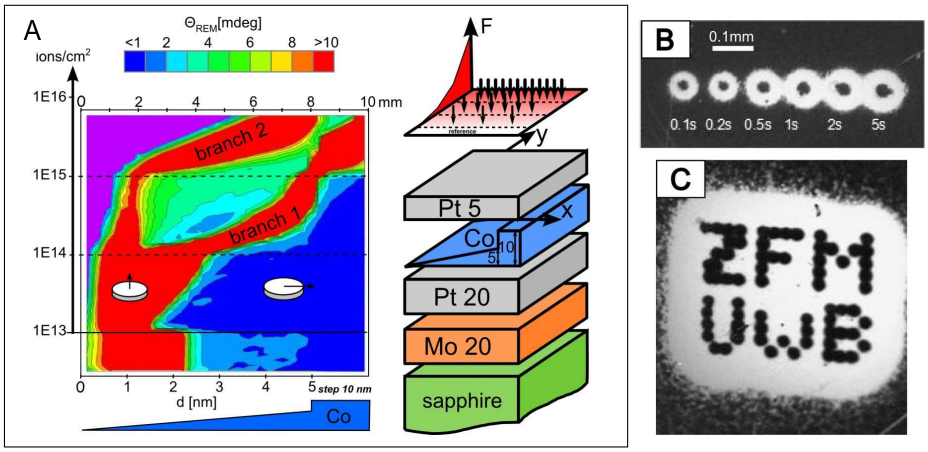

Fig. 8: P-MOKE-based remnant state in cobalt nanostructure, irradiated by: A) Ga^+ ions; $10 \times 10\,mm^2$ large sapphire substrate with Co wedge deposited along the "x" axis, sandwiched by Pt layers, gallium fluence F along the "y" axis (for y starting from 2 mm until 8 mm), and B), C) pulsed laser beam (pulse width = 140 fs, wavelength = 7, 00 nm, average power = 1.9 W, with a pulse repetition rate of 90 MHz [20]); spots with different illumination time (B) and an example of "writing" by light (C).

The influence of light pulses on Co magnetic ordering was studied on Au/Co/Au layers deposited by a UHV magnetron sputtering onto mica [20]. A low critical thickness d_{RPT} (about 0.9 nm) was observed in these films, so one can conclude that these films are characterized by little magnetic surface anisotropy. Laser pulses, focused on the sample, induced creation of the out-of-plane magnetization state – see white areas in Fig. 8B with $d > d_{\mathrm{RPT}}$. The laser-driven creation of the out-of-plane magnetization state is explained as the light-induced increase of the quality of Co-Au interfaces. The effect of laser beam modification of magnetic ordering was used for the preparation of an example of "writing" by light, see Fig. 8C.

Examples of Co nanostructures lateral patterning

By knowing methods for changing magnetic properties, one can use them for a patterning of magnetic nanostructure. An example of laser light patterning – "writing" is shown in Fig. 8B, C. The strong influence of both Au and Mo buffers on magnetic anisotropy (compare Mo/Co/Au and Au/Co/Au zones in Fig. 6) was used in a series of works [21, 22] for creation of magnetic dots in the form of Co deposited on Au islands, grown on a Mo layer. The ion-degradation of both magnetic anisotropy and coercivity was used to create, by He-ions-irradiation, the following: (i) a regularly arranged artificial magnetic out-of-plane pattern

(by the irradiation of an Au/Co/Au layer system through a colloidal mask of hexagonally-arranged spherical polystyrene beads [23]); (ii) a coercivity wall (by ion bombardment of (Co/Au) multilayers through a wedged Au stopper layer [24]). Especially promising seems to be the application of a gallium focused ion beam (FIB) for magnetic patterning, using the Ga-fluence-driven effects described in Ref. [4]. This gives opportunities for creation of new materials, e.g. new types of magnonic crystals.

4. Magnetization distributions in magnetic nanostructures

A review of the results of experimental and theoretical studies of single films, laterally patterned nanostructures, and multilayers, is presented. Generally, magnetization distribution in such systems is very complicated, and typical theories have to be based on many simplifications (neglecting e.g. the width of the domain wall, or magnetization distribution in sample thickness). Thus, micromagnetic simulations were performed, using OOMMF software [25]. Two material parameters are usually used for analysis of magnetization distributions: (i) quality factor $Q = K_1/(2\pi M^2)$ (i.e. the ratio of the anisotropy energy to be gained by magnetization along the easy axis perpendicular to the sample surface, and the magnetostatic energy of a uniformly magnetized layer along the surface normal) and (ii) exchange length, $l_{\mathrm{ex}}(l_{\mathrm{ex}} = (A/(2\pi M^2))^{0.5},\ A$ is the exchange constant). Our disussion is illustrated by simulations performed using material parameters taken (Q, l_{ex}, M) for cobalt samples.

Single films

There are different types of magnetic domains in nanostructures. Domain properties strongly depend on the relation between the coercivity field and the demagnetization field.

In the ultrathin region, far from the RPT, at low thickness, the coercivity field dominates the demagnetization one. Usually in this region one can observe: (i) a square hysteresis loop, (ii) magnetization-reversal aftereffects, (iii) "Swiss cheese" type domain structures – see an example in Fig. 9, (iv) nonreversibility of magnetization processes, and strong dependence of domain structure properties on a samples magnetic history [26, 27, 28]. In this case, the static and dynamic properties of magnetization distribution are described using a model concerning spatial changes of local coercive fields. Domain geometry depends on the distribution of magnetic defects and on the samples magnetic history.

Magnetostatic forces begin to be important while approaching the reorientation phase transition, either by increasing the thickness of the sample, d, (which results in a decrease in magnetic anisotropy, see Eq. 1, and a decrease in Q down to 1 while approaching d_{RPT}) or by applying an in-plane magnetic field. Let us

consider the domain period for cobalt, assuming the $Q(d)$ dependence reported in Ref. [10]. A drastic change of domain structure sizes (in the range of several orders of magnitude) has been determined, while approaching the thickness-driven RPT from an out-of-plane magnetization state to the in-plane one in the ultrathin cobalt layer – see the left curve in Fig. 10 with stripe domain period determined in a wide thickness range. Sinusoidal-like magnetization distribution was obtained from simulations [29], while approaching the RPT.

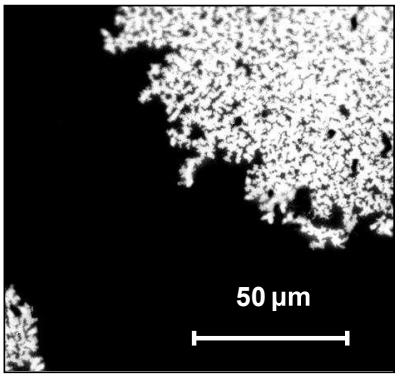

Fig. 9: Example of the "Swiss cheese" type domain structures.

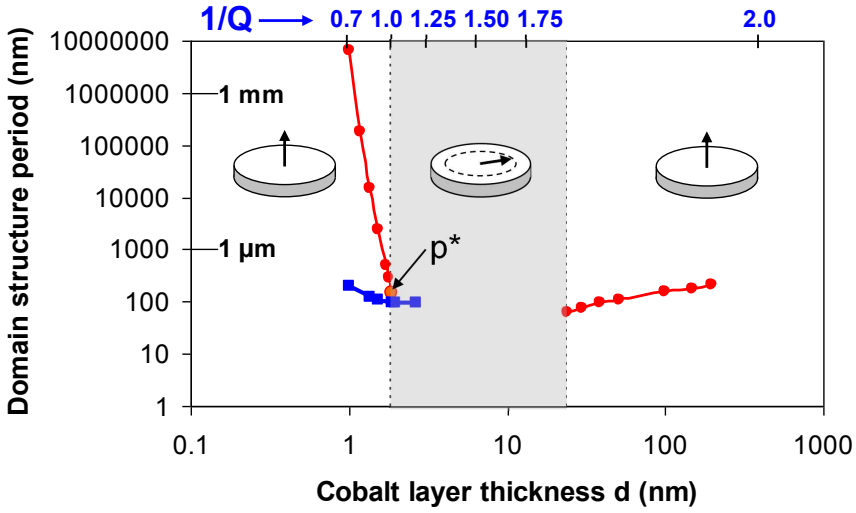

Fig. 10: Dependence of domain period as a function of Co layer thickness d determined for both single layer and double layer structures.

Assuming such simple magnetization distribution, we have calculated the following formula [29] describing the critical period of this domain structure:

$$p^* = 8\pi l_{\mathrm{ex}}^2/d + 2\pi d \tag{2}$$

where l_{ex} is the exchange length. Domain structure exists until quality factor reachs Q^* (corresponding to thickness d^*) slightly lower than 1, so there is an extended range of thicknesses in which the out-of-plane magnetization state, $d^* > d_{\mathrm{RPT}}$ exists. This solution stands for a universal description applicable to a wide class of ultrathin nanostructures.

A similar critical domain structure, with a period described by Eq. 2 is valid for RPT induced by an in-plane applied field. In this case, one can expect different metastable domain structures in ultrathin film, depending on the magnetic history of the sample, characterized by high enough coercivity to "freeze" these metastable structures. This expectation was confirmed by our experiments performed with 1 nm thick Co film [30], where large domains (1 mm size) and small domains (submicrometer size) were observed for a sample demagnetized by perpendicular and by in-plane magnetic applied fields, respectively.

While increasing d thickness above d^*, magnetization is in-plane oriented. However, above the second critical thickness, d_{RPT2}, magnetization distribution with out-of-plane magnetization components appears. Magnetization distribution is more complicated (dependent on its distance from the surface of the sample) than distribution for $d < d^*$. For cobalt, this second transition occurs for an approximately 20 nm thick layer. For $d > d_{\mathrm{RPT2}}$ we have determined magnetization distribution as stripe domains, more precisely as vortex-like stripe domains with in-plane-oriented vortex cores parallel to the stripes [31]. For this case the dependence of stripe domain period versus thickness is shown in Fig. 10 (right curve).

Multilayers

$(\mathrm{Co/NF})_N$ multilayers were investigated, where Co layers (with different thicknesses d and Q value) were separated by NF nonferromagnetic layers (with different thickness d_{NF}). N means the number of repetitions.

The interaction between two magnetic layers is important – one can find the influence of this interaction, compared with a single layer, on both (i) a decrease of the domain period and (ii) extension of the thickness range for which an out-of-plane magnetization state exists, see Fig. 10. The extended range of out-of-plane magnetization we determined [32] on the (Q, N)-phase diagram.

$(\mathrm{Co/Au})_N$ ultrathin multilayers with $Q > 1$ or $Q < 1$ (high or low magnetic anisotropy case) were studied experimentally [33] using a combination of ferromagnetic resonance, magneto-optical magnetometry and microscopy (with both in-plane and out-of-plane magnetization-sensitive longitudinal and polar Kerr ef-

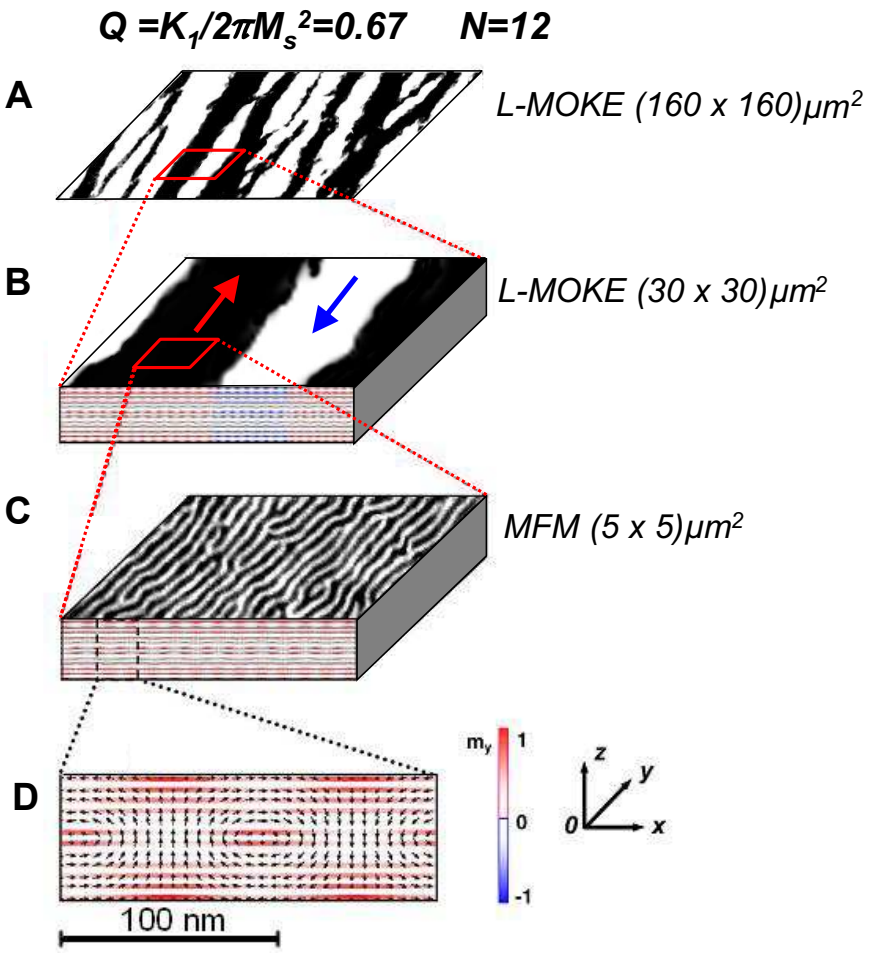

Fig. 11: Domain structure reconstruction in Co-Au multilayers (with $Q = 0.67$, $N = 12$ layers, $d = 2\,\mathrm{nm}$) based on L-MOKE, MFM images and simulations. Subsequent Fig. 11 parts are on a different scale: A) LMOKE image from $160 \times 160\,\mu\mathrm{m}^2$ large area; B) L-MOKE image from $30{\times}30\,\mu\mathrm{m}^2$; C) MFM image $5{\times}5\,\mu\mathrm{m}^2$; D) simulated area (considering $Q = 0.67$, $N = 12$), magnetization components m_x, m_z directions are defined by arrows; while the m_y component is defined by color. Dotted lines from upper to bottom images illustrate enlargement of investigated areas.

fects), and magnetic force microscopy (MFM). For $Q > 1$ we observed, when increasing N: (i) a strong change of the hysteresis loop connected with an increase of the saturation field and change of sign (from negative to positive) of the field of domain nucleation; (ii) a decrease of domain size. For $Q < 1$ we found then, while increasing N, the appearance of a domain structure with out-

of-plane magnetization. Fig. 11 shows magnetization distribution, reconstructed in both experiments and simulations. Large, micrometer sized domains with in-plane magnetization (visualized by L-MOKE) are "modulated" by submicometer sized domains (MFM imaging) with magnetization perpendicular to the plane. Fig. 11D shows the vortex-like magnetization distributions with vortex cores along its domain stripes – in the "y" direction.

5. Conclusions

It has been proven that our developed magneto-optical magnetometers are very powerful for studies of magnetic nanostructures e.g. analysis of magnetic and magneto-optical properties as a function of different parameters such as thicknesses of nanostructure components and irradiation fluence.

Very promising are new, just launched, methods for studies of magnetization dynamics, enabling studies in either time or frequency domains, with the opportunity to study a process in a wide time scale from quasistatic to femtosecond.

We have shown, in systematic combined studies, the influence of different factors on modification of cobalt magnetic and magnetooptical properties during both nanostructures deposition and post-growth processes. Especially interesting seem to be results showing different agents suitable for local tailoring of the magnetic anisotropy and the resulting existence of an out-of-plane magnetization state. We have developed descriptions, confirmed by experiments, of magnetization distribution and magnetization processes in a wide range of both nanostructures thicknesses and magnetic anisotropy. The results obtained look to be important for general knowledge and possible applications. These results can be used to create new artificial systems with desired magnetic properties and reduced dimensions down to the atomic scale. Particularly interesting are metallic magnetic nanostructures, combined with either semiconductors [34, 35] or dielectric [36] materials, which may be the key to create spintronic devices as well as patterned magnetic media. A new direction of our research has just been launched: the study of magnonic crystals. The theory of spin waves developed by the team from the Department of Surface Physics UAM from Pozna [37–39], is important for this research step for such studies.

Acknowledgment

Our teams study results for nanomagnetism have been published in 122 papers prepared under international cooperation (156 coauthors from 31 countries), including 79 papers that were prepared in the frame of the NANOMAG-LAB project coordinated by the Białystok team. The results of studies of nanomagnetism were the bases of three habilitation theses prepared in Białystok as well as some PhD theses prepared in Bialystok and in cooperating teams.

During all these years, we have fruitfully cooperated with Jacques Ferre. Discussions with Henryk Szymczak were very essential for us during our nanomagnetis studies. Very important was cooperation within the Polish network ART-MAG with mutually supporting research activities. Results of cooperation on studies of magnetic both metallic structures (with the teams of Tomasz Baczewski and Andrzej Wawro from Warsaw; Feliks Stobiecki from Poznań; Józef Korecki and Tomasz Stobiecki from Kraków) and semiconductors structures (with the team of Tomasz Dietl from Warsaw) have resulted in 65 common papers. We are grateful to Vitalii Zablotskii from Prague for his theoretical support.

Recent important developments of experimental techniques of our laboratories were achieved because of financial support of the EU programme Innovative Economy, Priority 2.2, No. POIG.02.02.00-00-020/09 SPINLAB. This work was partially supported by SYMPHONY project operated within the Foundation for Polish Science Team Programme co-financed by the EU European Regional Development Fund, OPIE 2007-2013.

References

[1] A. Stupakiewicz, A. Kirilyuk, A. Fleurence, R. Gieniusz, T. Maroutian, P. Beauvillain, A. Maziewski, Th. Rasing, Phys. Rev. B **80** (2009) 094423

[2] R. Gieniusz, T. Błachowicz, A. Maziewski, A. Petroutchik, L. Baczewski, A. Wawro, J. Hamrle, O. Serga, B. Hillebrands, Acta Physica Polonica A **115** (2009) 213–216

[3] J. Jaworowicz, A. Maziewski, P. Mazalski, M. Kisielewski, I. Sveklo, M. Tekielak, V. Zablotskii, J. Ferré, N. Vernier, A. Mougin, K. Postava, J. Fassbender, A. Henschke, Appl. Phys. Lett. **95** (2009) 022502

[4] A. Maziewski, P. Mazalski, Z. Kurant, M. O. Liedke, J. McCord, J. Fassbender, J. Ferré, A. Mougin, A. Wawro, L. T. Baczewski, A. Rogalev, F. Wilhelm, T. Gemming, Phys. Rev. B **85** (2012) 054427

[5] J. Kisielewski, A. Kirilyuk, A. Stupakiewicz, A. Maziewski, A. Kimel, Th. Rasing, L. T. Baczewski, A. Wawro, Phys. Rev. B **85** (2012) 184429

[6] F. Atoneche, A. M. Kalashnikova, A. V. Kimel, A. Stupakiewicz, A. Maziewski, A. Kirilyuk, Th. Rasing, Phys. Rev. B **81** (2010) 214440

[7] S. O. Demokritov, V. E. Demidov, in: Spin Wave Confinement, Pan Stanford Publishing Pte. Ltd., World Scientific Publishing Co. Pte. Ltd., 2009

[8] B. Hillebrands, J. Hamrle, in: Handbook of Magnetism and Advanced Magnetic Materials, Eds. H. Kronmuller, S.P. Parkin, (Wiley-Inter-science, UK 2007), Vol. 3, p. 1566.

[9] V. E. Demidov, H. Ulrichs, S. Urazhdin, S. Demokritov, V. Bessonov, R. Gieniusz, A. Maziewski, Appl. Phys. Lett. **99** (2011) 012505

[10] M. Kisielewski, A. Maziewski, M. Tekielak, A. Wawro, L. T. Baczewski, Phys. Rev. Lett. **89** (2002) 087203

[11] M. Kisielewski, A. Maziewski, Z. Kurant, M. Tekielak, A. Wawro, L. T. Baczewski, J. Appl. Phys. **93** (2003) 7628

[12] M. Tekielak, Z. Kurant, A. Maziewski, L. T. Baczewski, A. Maneikis, A. Wawro, J. Magn. Magn. Mater. **290–291** (2005) 783–786

[13] M. Tekielak, R. Schafer, J. McCord, A. Maziewski, V. Zablotskii, L. T. Baczewski, A. Wawro, J. Magn. Magn. Mater. **316** (2007) 184–187

[14] R. Gieniusz, L. T. Baczewski, Z. Kurant, A. Maziewski, A. Wawro, J. Magn. Magn. Mater. **310** (2007) 2198–2200

[15] Z. Kurant, R. Gieniusz, A. Maziewski, M. Tekielak, W. Stefanowicz, I. Sveklo, V. Zablotskii, A. Petroutchik, L. T. Baczewski, A. Wawro, J. Magn. Magn. Mater. **316** (2007) e511–e514

[16] A. Stupakiewicz, A. Maziewski, K. Matlak, N. Spiridis, M. Ślęzak, T. Ślęzak, M. Zając, J. Korecki, Phys. Rev. Lett. **101** (2008) 217202

[17] A. Stupakiewicz, E. Vedmedenko, A. Fleurence, T. Maroutian, P. Beauvillain, A. Maziewski, R. Wiesendanger, Phys. Rev. Lett. **103** (2009) 137202

[18] A. Stupakiewicz, A. Maziewski, M. Ślęzak, T. Ślęzak, M. Zając, K. Matlak, J. Korecki, J. Appl. Phys. **103** (2008) 07B520

[19] C. Chappert, H. Bernas, J. Ferre, V. Kottler, J.-P. Jamet, Y. Chen, E. Cambril, T. Devolder, F. Rousseaux, V. Mathet, H. Launois, Science **280** (1998) 1919

[20] J. Kisielewski, K. Postava, I. Sveklo, A. Nedzved, P. Trzciński, A. Maziewski, B. Szymański, M. Urbaniak, F. Stobiecki, Solid State Phenomena **140** (2008) 69

[21] A. Wawro, E. Sieczkowska, A. Petroutchik, L. T. Baczewski, Z. Kurant, A. Maziewski, Phys. Rev. B **83** (2011) 092405

[22] A. Wawro, A. Petroutchik, L. T. Baczewski, Z. Kurant, A. Maziewski, EPL **89** (2010) 37003

[23] P. Kuświk, A. Ehresmann, M. Tekielak, B. Szymański, I. Sveklo, P. Mazalski, D. Engel, J. Kisielewski, D. Lengemann, M. Urbaniak, Ch. Schmidt, A. Maziewski, F. Stobiecki, Nanotechnology **22** (2011) 095302

[24] M. Urbaniak, P. Kuświk, Z. Kurant, M. Tekielak, D. Engel, D. Lengemann, B. Szymański, M. Schmidt, J. Aleksiejew, A. Maziewski, A. Ehresmann, F. Stobiecki, Phys. Rev. Lett. **105** (2010) 067202

[25] M. Donahue, D. Porter, Object Oriented Micromagnetic Framework, http://math.nist.gov/oommf

[26] J. Ferre, V. Grolier, P. Meyer, A. Maziewski, E. Stefanowicz, S. V. Tarasenko, V. V. Tarasenko, M. Kisielewski, D. Renard, Phys. Rev. B **55** (1997) 15092

[27] M. Kisielewski, A. Maziewski, J. Ferre, V. Mathet, C. Chappert, Materials Science Forum **373–376** (2001) 121

[28] M. Kisielewski, A. Maziewski, M. Tekielak, J. Ferre, S. Lemerle, V. Mathet, C. Chappert, J. Magn. Magn. Mater. **260** (2003) 231–243

[29] M. Kisielewski, A. Maziewski, T. Polyakova, V. Zablotskii, Phys. Rev. B **69** (2004) 184419

[30] M. Kisielewski, A. Maziewski, V. Zablotskii, T. Polyakova, J. M. Garcia, A. Wawro, L. T. Baczewski, J. Appl. Phys. **93** (2003) 6966

[31] M. Kisielewski, A. Maziewski, V. Zablotskii, J. Magn. Magn. Mater. **316** (2007) 277

[32] M. Tekielak, M. Dąbrowski, M. Kisielewski, A. Maziewski, V. Zablotskii, J. Appl. Phys. **107** (2010) 083911

[33] M. Tekielak, R. Gieniusz, M. Kisielewski, P. Mazalski, A. Maziewski, V. Zablotskii, F. Stobiecki, B. Szymański, R. Schaefer, J. Appl. Phys. **110** (2011) 043924

[34] W. Stefanowicz, D. Sztenkie, B. Faina, A. Grois, M. Rovezzi, T. Devillers, F. d'Acapito, A. Navarro-Quezada, Tian Li, R. Jakieła, M. Sawicki, T. Dietl, A. Bonanni, Phys. Rev. B **81** (2010) 235210 15

[35] W. Stefanowicz, C. Śliwa, P. Aleshkevych, T. Dietl, M. Döppe, U. Wurstbauer, W. Wegscheider, D. Weiss, M. Sawicki, Phys. Rev. B **81** (2010) 155203

[36] M. Pashkevich, A. Stupakiewicz, A. Kirilyuk, A. Maziewski, A. Stognij, N. Novitskii, A. Kimel, Th. Rasing, J. Appl. Phys. **111** (2012) 023913

[37] J. O. Vasseur, L. Dobrzynski, B. Djafari-Rouhani, H. Puszkarski, Phys. Rev. B **54** (1996) 1043

[38] H. Puszkarski, M. Krawczyk, Solid State Phenomena **94** (2003) 125–134

[39] M. Krawczyk, H. Puszkarski, Phys. Rev. B **77** (2008) 054437

Received May 29, 2012